

Chapter 2

Microfluidic Methods in Single Cell Biology

Arnab Mukherjee and Charles M. Schroeder

Abstract Stochastic variations within seemingly homogeneous cell populations determine the emergent properties of complex cellular systems such as biofilms, tumors, pluripotent stem cells, and multispecies ecosystems. The advent of microfluidic technologies, coupled with rapid advances in fluorescence-based molecular imaging and genomic, transcriptomic, and proteomic profiling techniques, has spurred a revolution in biological analysis at the level of single cells. Over the past decade, several microfluidic platforms have been developed that enable the isolation, enrichment, and biochemical or genetic analysis of individual cells with high spatiotemporal resolution in a fashion that is not achievable using macroscale methods. In sharp contrast to population-averaged measurements based on bulk-level techniques, microfluidic cell culture platforms permit the acquisition of multiparametric and high-content information while preserving the identity and monitoring the behavior of individual cells over time. In this way, microfluidics has ushered in new frontiers in single cell biology with a direct impact on applied and foundational studies in microbial ecology, systems biology, therapeutics development, and clinical diagnostics. In this chapter, we describe the transformative impact of microfluidics in single cell biology with particular emphasis on the following areas: (1) microfluidic bioreactors for cellular analysis in dynamically changing microenvironments, (2) microfluidic chips for in vitro drug screening, and (3) single cell confinement and isolation microchips for sorting and profiling rare or unculturable cells in complex environmental consortia.

Keywords Biological noise • Stochasticity • Laminar flow • Antibiotic resistance • Single cell genome amplification • Circulating tumor cells • Unculturable microbes • Time-lapse fluorescent microscopy

A. Mukherjee, Ph.D.

Division of Chemistry and Chemical Engineering, California Institute of Technology, 1200 E. California Blvd., 123 Spalding, Pasadena, CA 91125, USA
e-mail: arnabm@caltech.edu

C.M. Schroeder, Ph.D. (✉)

Department of Chemical and Biomolecular Engineering, Center for Biophysics and Computational Biology, Institute for Genomic Biology/Biosystems Design, University of Illinois at Urbana-Champaign, 600 S. Mathews Avenue, Urbana, IL 61801, USA
e-mail: cms@illinois.edu

2.1 Introduction

2.1.1 *Single Cell Biology*

Cells are inherently noisy systems in that they exhibit significant off-mean excursions in protein and RNA levels even in isogenic populations and in homogeneous environments [1, 2]. The stochastic nature of gene expression and the resulting variations in cellular phenotypes are exemplified by several biological phenomena including microbial bet-hedging strategies to survive stressful environments, generation of drug-resistant tumor subpopulations, antibiotic persistence, aging, development of multifunctional phenotypes of cytotoxic tumor-infiltrating lymphocytes (CTLs), stem cell differentiation, and variable metastatic potential within a population of circulating tumor cells (CTCs) derived from the same tumor [1–11]. Stochastic fluctuations in gene expression are strongly affected by the architecture of the underlying genetic network and are particularly relevant at low concentrations of biomolecules. To this end, a quantitative resolution of cell-to-cell variations in gene expression and associated phenotypes for natural and engineered cellular systems constitutes a fundamental challenge for single cell biology [3, 4, 7]. Classically, biological noise has been studied using destructive end-point techniques such as fluorescence-activated cell sorting (FACS) or time-lapse fluorescence microscopy (TLFM) in combination with fluorescently labeled promoters, proteins, or RNA molecules (typically labeled using fluorescence in situ hybridization or FISH) [6, 12, 13]. FACS, however, is limited in its temporal resolution, while conventional TLFM is limited in the throughput and information content accessible from a single experiment. Furthermore, these approaches do not permit facile manipulation of the cellular microenvironment using precise spatiotemporal cues, which is critical for quantitatively interrogating single cell behavior.

2.1.2 *Microfluidic Approaches to Single Cell Biology*

Microfluidics broadly refers to the manipulation of picoliter to nanoliter-scale volumes of fluids in flow channels, reagent wells, and reaction chambers with dimensions ranging from a few to hundreds of micrometers [14–17]. Microfluidics enables miniaturization of biochemical reactions by a factor of 10^3 – 10^6 , which greatly improves the sensitivity (by enhancing signal to background) of conventional cellular and molecular biological assays, while also minimizing sample and reagent consumption and reducing the overall experimental footprint. Microfluidic devices are compatible with widely used assay readout technologies including fluorescence, luminescence, surface plasmon resonance, and even mass spectrometry. Importantly, fluid flow in microfluidic channels tends to be laminar (such that viscous forces dominate over inertial forces), which facilitates the creation of precise gradients in concentrations of reagents, thereby enabling spatially defined

manipulations with cellular to subcellular spatial resolution [14–21]. Heat exchange and mass transfer proceed rapidly owing to the large surface-to-volume ratios of microfluidic devices, which is useful for delivering dynamic temporal stimuli to cells. Finally, the small form factor associated with microfluidic devices provides a useful framework to realize multiplexed systems integrating multiple steps in cell biology including cell growth, sorting, lysis, and downstream analysis using quantitative PCR, FISH, and antibody labeling. Integrated microfluidic systems circumvent the need for off-chip procedures, thereby greatly improving speed and precision of biological assays [14, 22, 23]. Furthermore, automation can be readily achieved using inexpensive computer-controlled syringe pumps and air flow controllers, which obviates the need for cost-prohibitive robotic liquid handling systems.

2.1.2.1 Microfluidic Fabrication Techniques

Microfluidic systems can be constructed using a variety of materials including silicon, glass, polycarbonate, parylene, polystyrene, polymethyl methacrylate, water-in-oil droplets, and even paper [16, 24]. The material of choice for the vast majority of microfluidic cell handling platforms, however, continues to be a silicone elastomer—polydimethyl siloxane, commonly referred to as PDMS. PDMS offers unique advantages for biological applications including nontoxicity for cell growth, high gas permeability, optical transparency, and relative inertness to most reagents typically employed in cell culture. In addition, PDMS enables rapid prototyping of microfluidic devices using widely established soft lithographic procedures. In this technique, a microfluidic relief pattern is first patterned on a silicon wafer using a UV light source together with a photomask to spatially control light exposure on a layer of photoresist-coated silicon wafer to produce a master mold. Next, unpolymerized photoresist is dissolved away leaving behind a positive or negative relief pattern on the silicon wafer, known as the master mold. The master mold wafers are treated with a release agent (trichlorosilane) and spin coated with a mixture of degassed PDMS and a curing agent and thermally cured for several hours at 65–80 °C in order to polymerize the PDMS. Cured PDMS can be detached from the silanized wafer and bonded to a glass slide that has been rendered hydrophilic by exposure to oxygen plasma. In this way, a single master mold can be used to rapidly develop up to hundreds of PDMS chips using replica molding [24–27]. Active fluidic valves can be incorporated into PDMS-based microdevices by fabricating multilayer chips, wherein PDMS layers are bonded to each other via plasma treatment [24, 25, 28–30]. Typical multilayer microfluidic devices consist of a fluid layer comprising the microfluidic channel network and arrays of reagent chambers sandwiched between PDMS and glass. Importantly, the low Young's modulus of PDMS can be exploited to enable facile on-chip fluid routing through the use of microfluidic valves, which can be pneumatically or hydraulically actuated. In this approach, a second PDMS layer known as the control layer is aligned and bonded above the fluidic layer. The control layer houses air flow lines that

enable the regulation of fluid flow in the fluidic layer by pushing (actuate-to-close vales) or pulling up (actuate-to-open vales) on the underlying PDMS layer at the intersection points of the control and fluid layers [28, 31]. Furthermore, by assembling and actuating valves in specified sequences or programs, peristaltic or rotary pump action can be achieved on-chip. Indeed, soft lithography can be recognized as the single most important factor responsible for the pervasive application of microfluidics by facilitating rapid design-to-prototype transition without the labor and expense associated with silicon microfabrication [16–18, 20, 21, 23–27, 30–32].

In the past decade, the vast majority of conventional macroscale technologies employed in cell and molecular biology studies has been micro-engineered and translated to microfluidic systems. This has led to the development of microfluidic cell sorters, electrophoresis platforms, patch clamps, on-chip thermal regulators, gradient generators, continuous and batch-mode cell culture systems, size-exclusion filters, and cell traps. Recently, microfluidic total analysis systems have been developed as miniaturized, self-contained platforms for cell culture and downstream chemical cytometry [14, 17, 20, 21, 25]. In this chapter, we present a broad overview of major advances in microfluidic applications for single cell biology. In order to highlight the transformative impact of microfluidics, we focus on key applications of novel microfluidic designs in first-of-its-kind studies in synthetic biology, environmental microbiology, and therapeutics development. Specifically, in Sect. 2.2, we describe the development and application of microfluidic bioreactors and single cell traps for investigating temporal patterns in gene expression. In Sect. 2.3, we review the application of microfluidics for developing complex spatial gradients in order to interrogate cellular phenotypes and gene expression in dynamic microenvironments. In Sect. 2.4, we discuss the extension of microfluidics platforms for high throughput and high content in vitro drug screening. Finally, in Sect. 2.5, we shift focus from microfluidic chips for single cell studies to microfluidic platforms that enable single species isolation and analyses. Here, we describe microfluidic devices that have been designed to isolate and profile rare cells (e.g., unculturable microbes) from heterogeneous and multispecies consortia. A unifying theme in the applications described in this chapter is the critical need for single cell isolation and/or characterization, which is uniquely enabled through the application of microfluidic technologies.

2.2 Microfluidic Platforms for Studying Gene Expression

An overarching goal of synthetic and systems biology is to achieve a quantitative understanding of gene expression and cell signaling pathways underlying cellular response in various conditions [14, 20]. At the heart of this approach is the ability to develop rigorous models of transfer functions that map a genetic network's output to a set of input stimuli. Experimentally, this is achieved through the application of defined perturbations to cells followed by a readout of cellular phenotype, typically

using fluorescent reporters [3, 7, 12, 13]. Microfluidic lab-on-a-chip platforms provide an ideal test bed for developing and testing such transfer functions because they enable precise and reproducible spatiotemporal control over the cellular microenvironment along with single cell resolution in experimental readout (e.g., using TLFM). Microfluidic approaches have several potential advantages compared to widely used microtiter plate-based assays, flow cytometry, and microarrays, in that microfluidics combines the benefits of fine-scale spatial and temporal control over the cellular microenvironment while alleviating the ensemble-averaging effects of population based assays. For these reasons, microfluidic chips have been extensively used for functional interrogation of engineered or natural genetic circuits in single isolated cells as well as in cell populations subjected to dynamic gradients in space and time [14, 20, 21]. In the following sections, we describe a few seminal studies in systems and synthetic biology that have leveraged the aforementioned benefits of microfluidic technologies.

2.2.1 *Microfluidic Dial-a-Wave Chip*

A prolific example of the integration of microfluidics and synthetic biology is afforded by the dial-a-wave microfluidic chip designed by Hasty and coworkers [33]. In this design, a population of yeast cells is constrained to grow as a monolayer in a microfluidic chamber, which is connected to feeding channels that supply the cells with nutrients and media (Fig. 2.1). Importantly, the composition of the media can be dynamically tuned using an upstream fluidic switch, which enables the generation of a wide range of stimulus waveforms. The fluidic switch was implemented using the principle of laminar interface guidance in which the laminar interface between two parallel flow streams can be precisely modulated by adjusting the respective flow rates. Hasty et al. used laminar interface guidance to control the composition of the input stream by varying the relative pressure (and thus the flow rates) between two reservoirs feeding the input lines (Fig. 2.2). Downstream of the inlets, complete mixing of the laminar flow streams was achieved using chaotic advection mixers that utilize the Coanda effect. In this way, a sinusoidal waveform of glucose concentrations (ranging from 0 to 0.25 %) against a background of constant galactose concentration (0.2 %) was generated and fed to the cell chambers. Strikingly, the authors demonstrated that the yeast cells respond to dynamic fluctuations in glucose concentrations by acting as low-pass filters, essentially filtering out nutrient fluctuations at frequencies exceeding 0.2 mHz (5.6 rad h^{-1}) (Fig. 2.3).

2.2.2 *Microfluidic Chemostat*

A persistent issue with microfluidic cell growth chambers is the clogging of microfluidic wells and flow lines by rapid cell growth and biofilm formation.

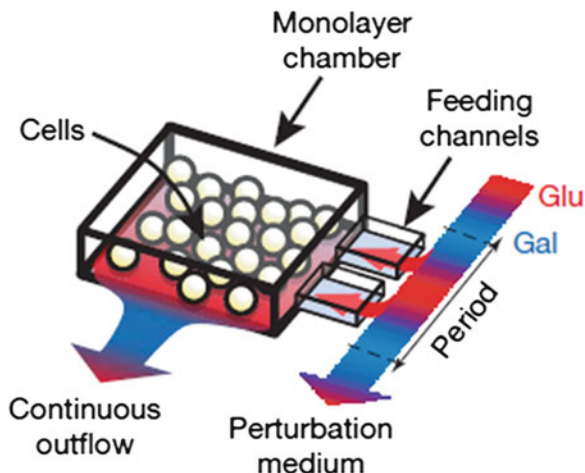


Fig. 2.1 Microfluidic dial-a-wave. The microfluidic dial-a-wave chip can be used to expose a monolayer of yeast cells to precisely defined waveforms in nutrient concentrations via feeding channels that connect the cell growth chamber to a flow channel perfused with media. In this example, Hasty et al. employed the dial-a-wave chip to subject cells to sinusoidal oscillations in glucose concentrations against a constant background of galactose. Reproduced with permission from Ref. [33]

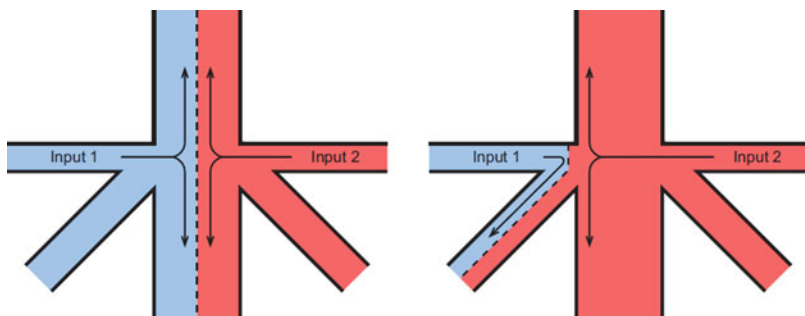


Fig. 2.2 Principle of laminar interface guidance. Laminar interface guidance works by guiding the interface between two laminar input flow streams, across an output channel by adjusting the relative flow rates of the input streams (stream 1 and stream 2 in the above illustration). In the microfluidic dial-a-wave, the flow rates were adjusted by controlling the pressure difference between the source reservoirs feeding input streams 1 and 2. Reproduced with permission from Ref. [33]

With a view toward addressing this issue, Quake and coworkers developed a highly integrated microfluidic chemostat for synthetic biology applications [34]. The microchemostat features 6 nL cell growth chambers where each growth chamber is essentially a microfluidic loop that employs on-chip peristaltic pumps to circulate cells at flow velocities of $250 \mu\text{m s}^{-1}$. Each growth chamber was further divided into 16 individually addressable segments. Through the implementation of on-chip

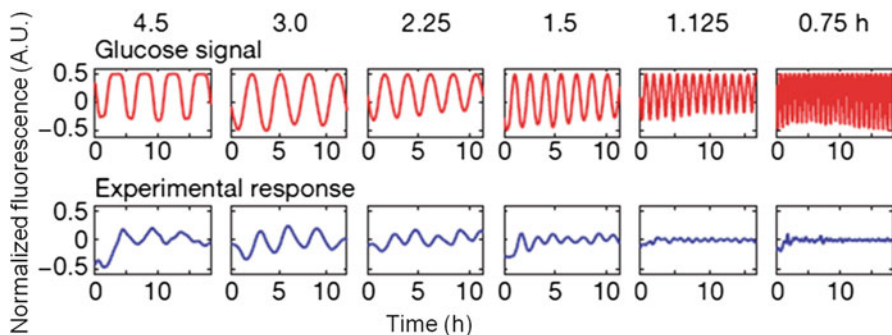


Fig. 2.3 Low-pass filtering action of yeast cells to dynamic fluctuations in glucose concentrations. As the frequency of oscillations in glucose concentrations is increased, the cellular response (quantified as normalized fluorescence on the y-axis) dies out indicating the robust filtering out of high frequency oscillations. Reproduced with permission from Ref. [33]

valves, each segment could be periodically isolated from the rest of the growth loop and washed with lysis buffer and sterile media in order to remove cells including wall-adhering biofilms. In principle, this step served as the microfluidic equivalent of continuous mode operation of a macroscale chemostat. Using the microchemostat, the authors demonstrated robust cell growth at dilution rates ranging from 0.072 to 0.37 h^{-1} . Importantly, the authors leveraged the microchemostat to sustain robust oscillations in a population of *E. coli* cells that had been genetically engineered to express a population control circuit. Specifically, *E. coli* cells were engineered to produce a quorum-sensing molecule (acyl homoserine lactone or AHL), which in turn could activate a toxic *ccdB* gene in a concentration-dependent manner. Consequently, as cell density increased in the microchemostat, the killer circuit was activated leading to a rapid decline in cell growth. Once the AHL concentrations dropped, the cells could resume growth again. Although several platforms for mimicking chemostat-like conditions on-chip have been described in recent times, the microchemostat by Quake and coworkers remains as one of the most intricate microfluidic cell culture platforms that accurately replicates chemostat-like conditions and enables long-term cell culture.

2.2.3 Microfluidic “Pin-Ball” Traps for Single Cells

Microfluidic live cell culture platforms such as the chemostat can be readily adapted for quantifying gene expression with single cell resolution over a statistically significant number of cells. In some applications, however, it is desirable to track gene expression or phenotype in a single cell over an extended duration, for example, in studies on cell aging or antibiotic persistence. Microfluidic

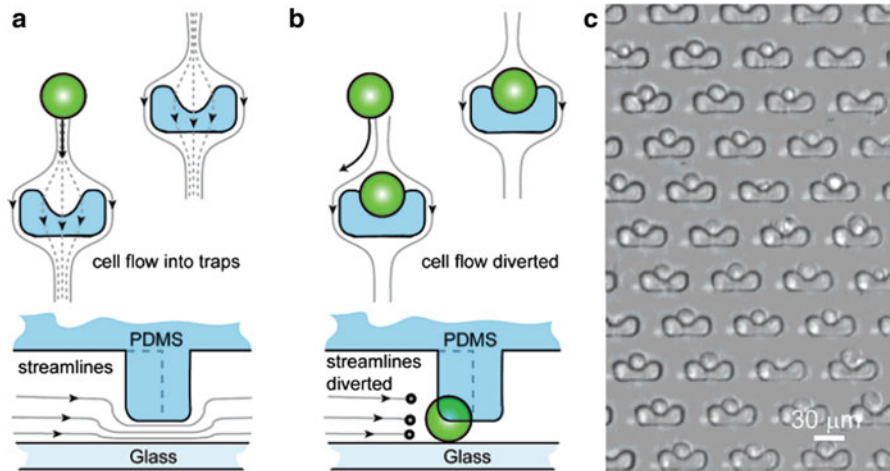


Fig. 2.4 Microfluidic pinball trap for single cells. (a) The pinball trap features cup-shaped PDMS obstacles that reduce the channel height to 2 μm at the trapping zones. In the absence of cells, fluid can flow freely through the reduced channel gap. (b) Upon encountering a PDMS post, a single cell becomes trapped because the channel height is three to fourfold smaller than the diameter of typical eukaryotic cells. Fluid flow is diverted around a cell trapped at the PDMS post, thereby forming an effective seal at the trapping zone. (c) Several PDMS posts are designed on a single chip to develop a single cell trapping array. Reproduced with permission from Ref. [35]

technologies for flow-based cell trapping avoid the need for potentially perturbative cell surface bonding approaches using electrostatic interactions or via chemical cross-linking. To this end, Lee and colleagues developed a microfluidic single cell isolation array that uses cup-shaped PDMS obstacles to function as physical barriers for trapping cells flowed into the device, in a fashion reminiscent of capturing balls in a game of pinball [35]. In this design, cells were flowed in through 40 μm high channels towards the trapping region that featured an array of suspended PDMS obstacles, which reduced the channel height to 2 μm (Fig. 2.4a). As the channel height at the trapping post is significantly smaller than the typical eukaryotic cell diameter (10 μm), cells were hydrodynamically trapped against the suspended PDMS obstacles. Trapping of a cell against a PDMS pillar effectively sealed the 2 μm high channel leading to highly efficient isolation of single cells at each trapping zone (Fig. 2.4b). Furthermore, the depth of the trapping pocket could be varied to tune the number of cells trapped in each obstacle, with greater than 50 % of the traps harboring single cells for a 10 μm deep pocket. Each microchip featured ~ 3300 PDMS obstacles per mm^2 of the device, which enabled the isolation of several cells on a single chip (Fig. 2.4c). The authors employed the microfluidic trap to isolate single HeLa, 293T, and Jurkat cells. Using this approach, the authors quantified for the first time, intracellular enzymatic activity of carboxylesterases using a fluorogenic substrate [35].

2.2.4 Microfluidic Yeast “Jails”

In order to quantify stochastic variability in the expression of genes implicated in aging in yeast, the ability to track a single yeast mother cell over several cycles of budding is critical. Rley and Pereira-Smith achieved this by designing PDMS yeast jails to physically trap a yeast cell $>4.5\ \mu\text{m}$ in diameter [36]. Optimal trapping of single cells was achieved using square-shaped PDMS posts arranged to enclose a space approximately $4.5\ \mu\text{m}$ wide. Asymmetric cell division of a mother cell trapped in between the square posts resulted in the budding of a daughter cell of diameter $< 4.5\ \mu\text{m}$, which could escape through the jail bars while the parent cell remains trapped (Fig. 2.5). Using the microfluidic yeast jail array, the authors demonstrated up to 92 % cell-to-cell variations in the levels of the RAS2 in yeast cells trapped and observed via TLFM for 18 h. As RAS2 overexpression has been demonstrated to enhance yeast life span by 20–40 %, the cell-to-cell variations in RAS2 levels observed by the authors could explain variations in life spans previously observed in isogenic yeast cell populations [36].

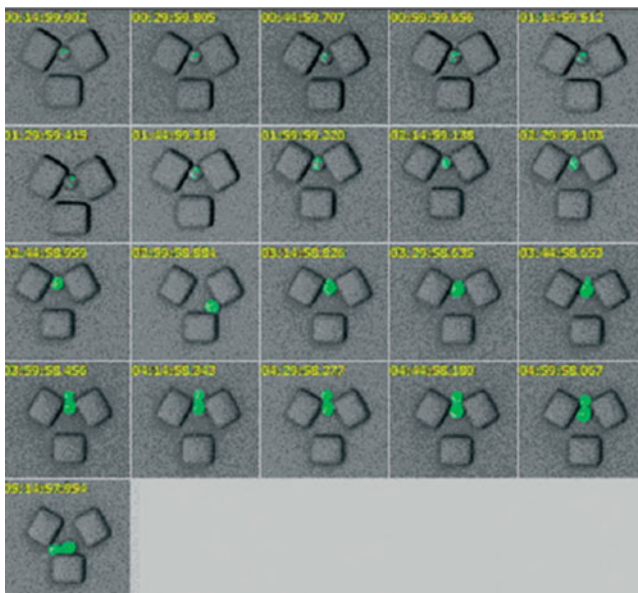


Fig. 2.5 Microfluidic yeast jails. A mother cell ($>4.5\ \mu\text{m}$ in diameter) is effectively trapped between the walls of the PDMS blocks, though it is free to move within the space enclosed by the PDMS posts. As the mother cell buds and produces a daughter cell, the smaller daughter cell is able to squeeze in through the gaps between the PDMS pillars leaving the mother cell isolated. Reproduced with permission from Ref. [36]

2.2.5 Single Cell Microbioreactor

A common feature of the vast majority of microfluidic traps involves the mechanical confinement of cells in PDMS microstructures (such as narrow grooves, jails, posts) fabricated on-chip. In contrast, our group reported the development of a contact-free microfluidic confinement approach for single cells and particles [37–39]. Our single cell microbioreactor (SCM) is a two-layered microfluidic device with the lower (fluidic) layer housing two inlet channels that converge at a $60\ \mu\text{m}$ deep cross-slot and diverge through two orthogonal outlet streams, thereby resulting in an extensional flow at the cross slot. As a result, a stagnation point (or point of zero fluid velocity) develops at the cross-slot, and the position of the stagnation point can be precisely regulated along the direction of extensional flow (i.e., the outlet direction) using on-chip valves located above the outlet streams in the control layer (Fig. 2.6). Cells are introduced in the cross-slot through a separate

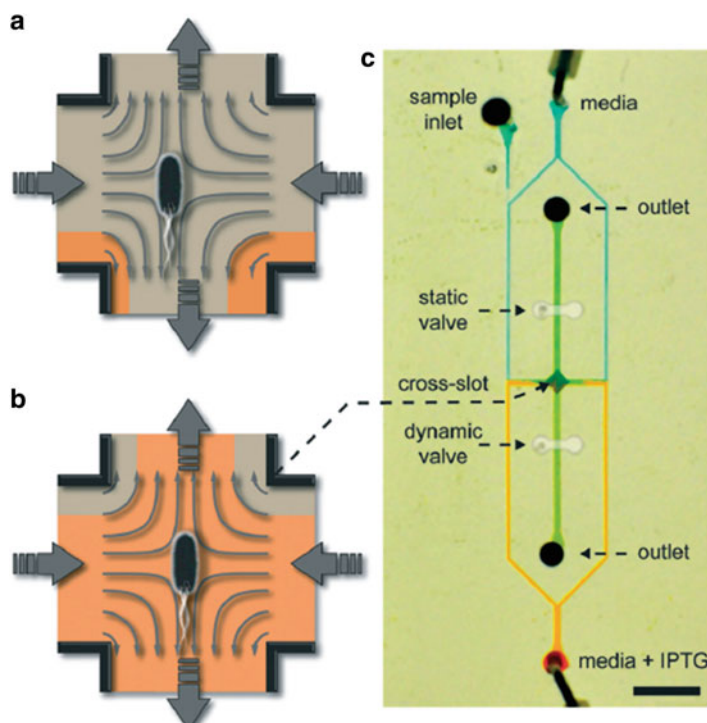


Fig. 2.6 Single cell microbioreactor. (a) The single cell microbioreactor traps individual cells in free solution at the saddle point of an extensional flow established in a microfluidic cross-slot. (b) Rapid media switching is achieved by changing the composition of the fluid flow in the inlet streams using programmable syringe pumps. (c) Micrograph of the single cell microbioreactor showing the fluid flow layers (filled with food coloring) and the control valves (in white) that are used to control the position of the stagnation point to actively maintain a cell in the trapping zone. Reproduced with permission from Ref. [39]

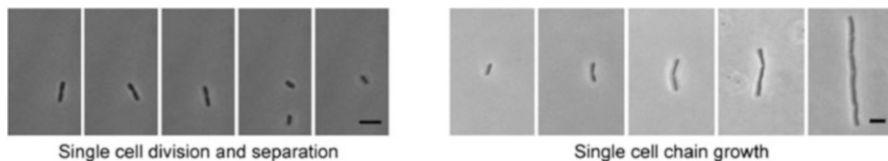


Fig. 2.7 Cell division and growth in the single cell microfluidic reactor. Single cells that were hydrodynamically trapped at the cross-slot are observed to grow and divide normally in case of cells harvested from exponentially growing cultures. In some cases, particularly for cells harvested from late stationary phase cultures, linear microcolonies resulting from chain-like growth were seen to develop at the cross-slot. Reproduced with permission from Ref. [39]

inlet stream connected to one of the input lines. Robust and long-term trapping (>3 h) of single cells at the cross-slot is achieved using a proportional feedback controller that pneumatically regulates pressurization and depressurization of the on-chip valve to precisely manipulate the position of the stagnation point within the cross-slot. The microfluidic SCM was used to quantify cell elongation and division rates in *E. coli* cells. Interestingly, we observed that single cells of *E. coli* adopt a filament-like growth morphology (where cells string up without splitting) when the mother cell is derived from a stationary phase culture whereas mother cells from exponential cultures symmetrically divide into two daughter cells (Fig. 2.7). A key advantage of the SCM is the ability to rapidly deliver nutrients and reagents on demand using automated programmable syringe pumps at the two inlets, which can be programmed to deliver precise stimulus waveforms. Media switching is accomplished significantly faster (≈ 1 s) compared to macroscopic methods for buffer exchange and other existing microfluidic cell culture chips, many of which rely on diffusive rather than convective mixing to accomplish fluid exchange. Using our approach, we investigated reporter gene expression in *E. coli* cells treated with a step increase in inducer (isopropyl thiogalactopyranoside or IPTG) concentration as well as a periodic square-wave form of IPTG concentration. We demonstrated that cellular response to a periodic forcing function differs from its response to a step function with respect to a delayed onset of gene expression as well as a slower rate of expression in the former case. Finally, we demonstrated that the SCM could be used to observe protein–DNA interactions in single cells and in real time. Specifically, *E. coli* cells were engineered to express the TetR repressor fused to a fluorescent protein and localized to a tandem TetR operator sequence array integrated in the chromosome. Focal spots of fluorescence localized at the chromosome could be clearly identified in single cells trapped at the cross-slot. Upon rapid (≈ 9 s) stimulation with anhydrotetracycline, the fluorescently tagged TetR proteins could be observed to unbind from the DNA and diffuse throughout the cytoplasm (Fig. 2.8) [39]. Overall, the SCM enables highly precise estimation of the time points of intracellular protein unbinding and diffusion, and we anticipate that the SCM can be a valuable tool for probing intracellular dynamics with exquisite temporal resolution.

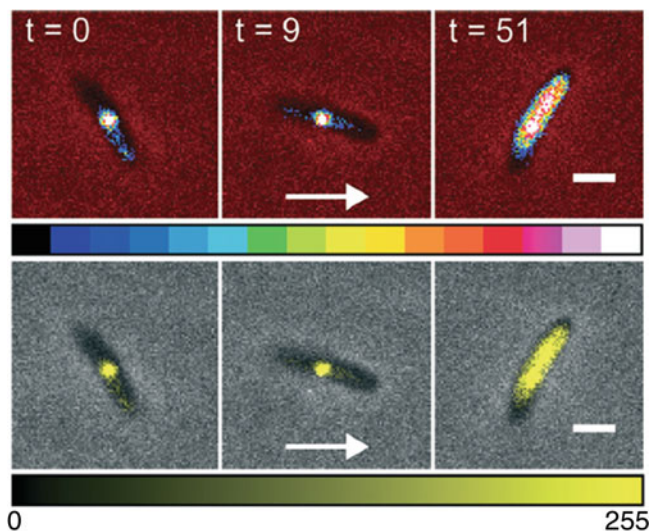
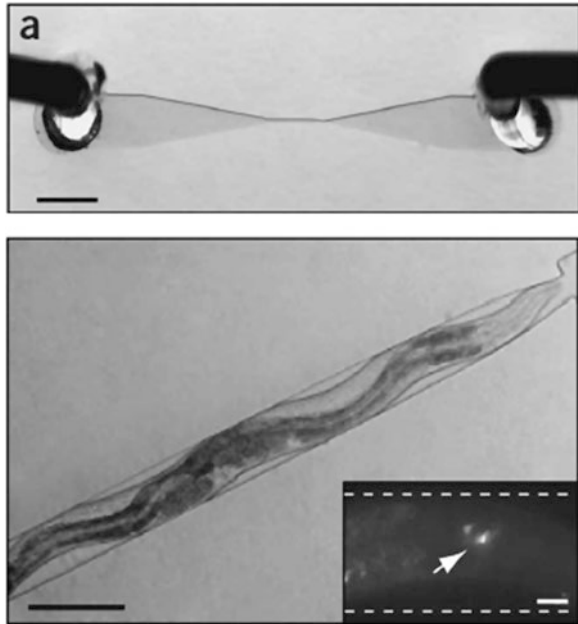


Fig. 2.8 Fluorescently tagged TetR proteins are observed to localize at the tetO binding array in the chromosome in a single trapped *E. coli* cell ($t = 0$ s). In approximately 9 s, the cell was treated with anhydrotetracycline (aTc) by rapid media switching. aTc binds to the TetR protein and causes it to unbind from its binding site at the DNA. At $t = 51$ s, the unbound TetR is seen to freely diffuse throughout the cell cytoplasm. Reproduced with permission from Ref. [39]

2.2.6 Microfluidic Worm Trap

Although the focus of the chapter is on single cells, we note that microfluidic traps have also been used to trap and study nematodes, zebrafish, and fly embryos [40–43]. For example, Chronis and colleagues described a microfluidic device that featured tapering channels, which gradually decreased in width from 70 to 40 μm and enabled trapping young adult worms by slightly constricting the thickest part of the worm body while leaving the head and tail free (Fig. 2.9) [43]. Microfluidic worm traps such as the one described by Chronis et al. are less perturbative than existing trapping techniques that employ potentially toxic glues to seal the worm head to agar supports. The gently compressed worms in the microfluidic trap retained the ability to propagate anterior and posterior traveling sinusoidal body waves. In addition, the authors demonstrated that anterior traveling body waves (which correspond to backward locomotion during crawling on agar plates) coincided with peaks in calcium concentrations in the AVA interneurons. The same work also described an olfactory chip that was used to locally stimulate the chemosensory neurons in the olfactory region of a trapped worm to varying stimuli (Fig. 2.10). The microfluidic device comprised four flow channels to subject the worm head to stimulus or buffer solutions (Fig. 2.10a, b). Fluidic switching between stimulus and buffer was achieved using two control channels on the side that delivered dye filled fluids to push the buffer or stimulus flows toward or away

Fig. 2.9 Microfluidic worm behavior chip. A young adult worm is trapped at the constriction zone of a microfluidic channel using gentle constriction applied at the thickest part of the worm body. The worm head and tail are free to move. (*inset*) Fluorescence expression from a calcium indicator (GCaMP) could be readily detected in the worm AVA interneurons and correlated with the development of an anterior traveling wave along the worm body. Scale bars: 1 mm, (*inset*) 20 μm . Reproduced with permission from Ref. [43]



from the worm head toward an outlet (Fig. 2.10c). Using the olfactory chip, the authors demonstrated calcium-dependent increase in fluorescence of a calcium sensor expressed in the ASH neurons of the worm upon the delivery of 15 and 30 s square pulses of a hyperosmotic stimulus.

2.3 Microfluidic Platforms for Generating Spatially Controlled Microenvironments

Although the microfluidic platforms described above are well suited for delivering temporal variations in stimuli, a key appeal of microfluidic platforms for single cell studies relies on the ability to generate highly precise and complex spatial gradients of soluble and surface-adsorbed molecules [19, 21]. Both microbial and eukaryotic cells frequently encounter complex spatial gradients in their native niches, which can be accurately recreated using microfluidics. From this perspective, the ability to generate controlled spatial microenvironments is critical for advancing fundamental understanding of several physiological processes such as chemotaxis in immune cells and bacteria, wound healing, inflammation, cancer metastasis, axonal growth, and stem cell migration. In the next few sections, we describe commonly used microfluidic gradient generators for cell biology studies.

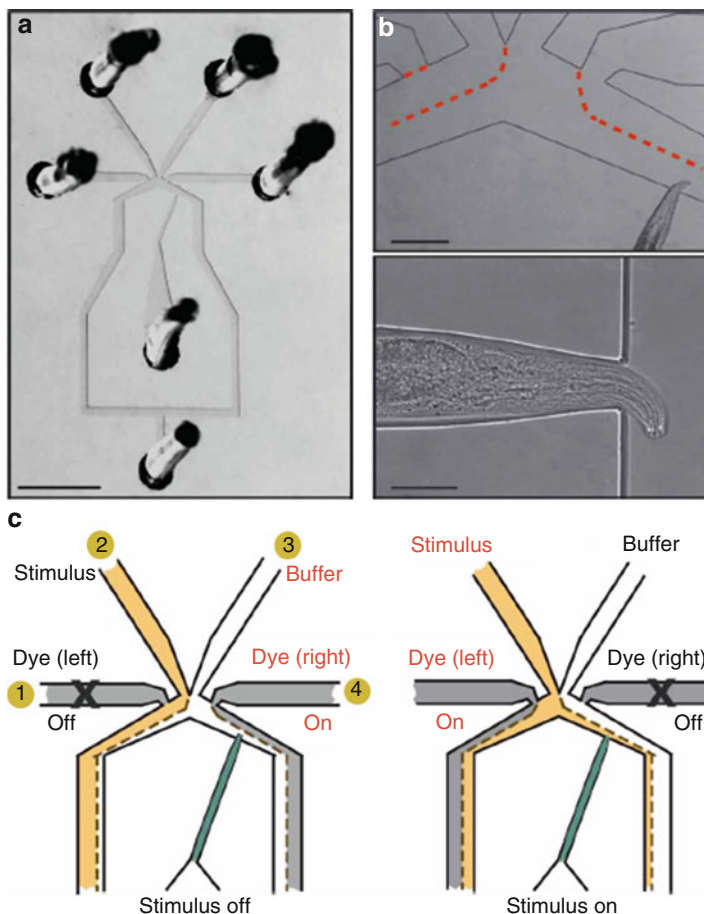


Fig. 2.10 Microfluidic olfactory chip. The microfluidic olfactory chip has four flow lines that (a) flow in media to (b) subject the head of a trapped worm to a defined odorant. (c) Rapid switching between stimuli is achieved via two flow lines on the side that are used to redirect stimulus toward or away from the trapped worm. Reproduced with permission from Ref. [43]

2.3.1 Microfluidic PARTCELL

Concentration gradients in space are typically generated by exploiting the laminar nature of microfluidic flows, which permits fluid streams containing different concentrations of reagents to flow in parallel over several hundreds of micrometers with minimal diffusive mixing. Parallel laminar flow streams can therefore result in stable gradients perpendicular to the flow direction. Flow rates required to maintain stable gradient shapes in microfluidic channels can be determined by the Peclet number, which quantifies the ratio of convective to diffusive flows and is determined by the flow velocity, channel geometry, and the diffusion coefficient of the molecules in question. Furthermore, laminar flow also allows the width of each of the parallel

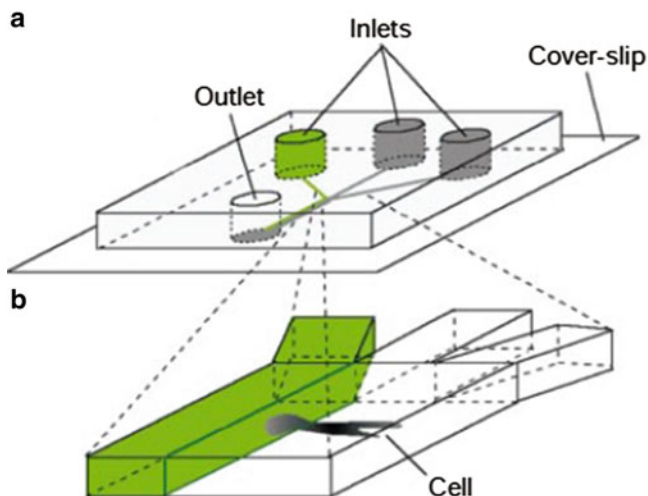


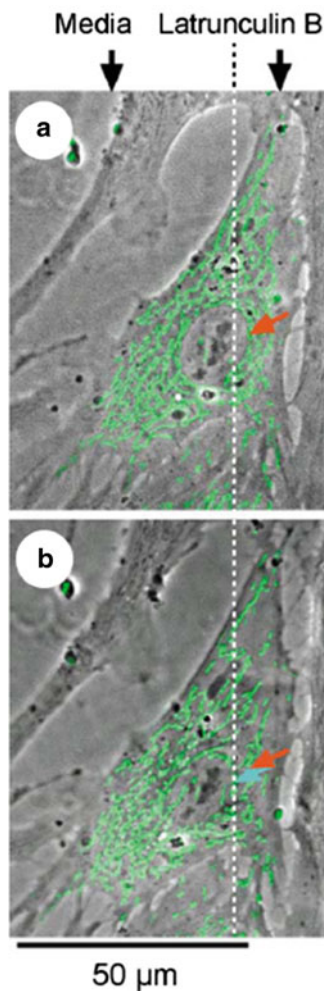
Fig. 2.11 Microfluidic PARTCELL. (a) A Y-shaped channel is used to establish parallel laminar flows of different reagents through multiple inlets. (b) The parallel streams, which mix minimally owing to the laminar flow regime, result in a concentration gradient perpendicular to the direction of flow. A cell adhered to a cover slip is subjected to the concentration gradient resulting in spatially selective exposure of the cell to various reagents. Reproduced with permission from Ref. [44]

streams to be precisely controlled by adjusting the relative flow rates, thereby enabling an unprecedented degree of spatial control over length scales typical of most eukaryotic cells (10–50 μm) [14, 16, 29]. Whitesides and colleagues first demonstrated this principle by developing the microfluidic PARTCELL (partial treatment of cells using laminar flows) to selectively treat a part of a surface attached to a bovine capillary endothelial (BCE) cell with various dyes and chemicals [44, 45]. In brief, Takayama et al. used a Y-shaped microfluidic channel to flow in two reagents in parallel streams over a surface-anchored BCE cell located $\approx 50\text{--}300\ \mu\text{m}$ downstream from the fluid inlets (Fig. 2.11). At these length scales, the width of the interface ranged between 1 and 10 μm . PARTCELL was used to selectively label mitochondria on each side of the cell with different colored dyes. Progressive intracellular mixing of the dyes throughout the cell was observed to proceed at rates determined by the intracellular diffusion coefficient of the dye ($\approx 1\ \mu\text{m}^2\ \text{s}^{-1}$). Interestingly, the same work also demonstrated spatially localized disruption of the cellular cytoskeleton by exposing the right side of the cell to latrunculin B, which is a membrane permeable actin-disrupting molecule (Fig. 2.12).

2.3.2 Y-Step Temperature Gradient Generator

Ismagilov and colleagues leveraged the Y-shaped microfluidic gradient generator design described above to develop temperature gradients across a *Drosophila* embryo attached to the floor of a microfluidic chip [40]. In particular, the authors

Fig. 2.12 Spatially selective cell treatment using PARTCELL. (a) A bovine capillary endothelial cell is adhered to the surface and treated with media flowing in parallel laminar streams. Mitochondria are labeled green and the nucleus is labeled with an arrow. In (a), the composition of both media streams is the same. In (b), the media on the right side of the cell is supplemented with latrunculin B, which disrupts the cellular actin cytoskeleton on the right side resulting in relocation of the mitochondria and the nuclei toward the left of the cell. The relocated position of the nucleus is indicated by a *blue arrow*. Reproduced with permission from Ref. [44]



employed the Y-shaped microfluidic gradient generator to flow two converging streams of liquid maintained at different temperatures, thereby subjecting each half of the *Drosophila* embryo to a different temperature (Fig. 2.13). Thermal diffusion across the 500 μm wide embryo was calculated to be limited to ~50 μm. In addition, most of the heat was lost through the 1.5 μm thick eggshell, resulting in the development of a tight step gradient in temperature across the width of the embryo. By introducing two parallel streams maintained at 20 °C and 27 °C, the authors demonstrated that the warmer half of the embryo developed more rapidly as evinced by the greater nuclear density in the warmer region of the embryo. Next, the authors followed dynamic expression of a key *Drosophila* developmental gene (known as even-skipped) in the embryo subjected to the 20–27 °C step gradient in temperature. In normally developing embryos, the even-skipped gene expression

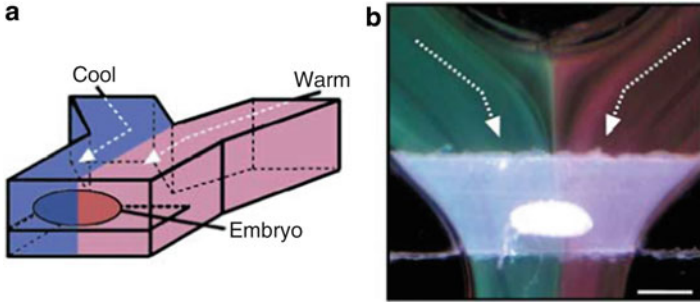


Fig. 2.13 Microfluidic temperature gradient generator. (a) By flowing cool and warm media through a Y-shaped microfluidic channel, Ismagilov and colleagues were able to subject a surface-attached *Drosophila* embryo to a step temperature gradient across the anterior–posterior axis of the embryo. (b) The temperature gradients were visualized using thermochromic crystals. The green stream is at 21 °C and the red stream is at 24 °C. Reproduced with permission from Ref. [40]

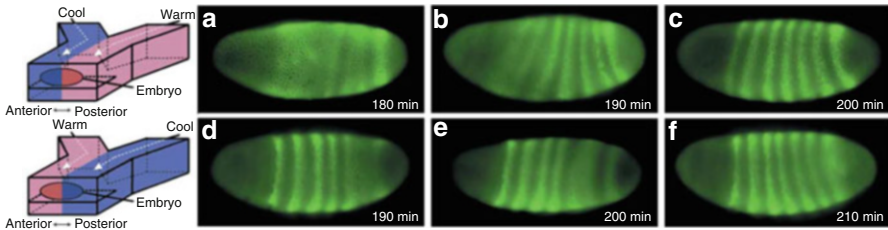


Fig. 2.14 Expression of a *Drosophila* developmental gene (known as even-skipped) in embryos subjected to a temperature gradient. Even-skipped gene expression (revealed by the striated fluorescent patterns) was found to develop preferentially in the warmer half of the embryo first. Strikingly, despite the deviation in the timing of even-skipped gene expression compared to a normal embryo, the final expression pattern was consistent with embryos maintained at a uniform temperature, pointing toward a regulated compensatory mechanism in cells. Reproduced with permission from Ref. [40]

results in a striped pattern across the length of the embryo with the stripes appearing in a precise temporal order. Strikingly, Luchetta et al. demonstrated that stripes resulting from the even-skipped gene expression consistently developed in the warmer half of the embryo first, although eventually the stripes developed across the embryo in a normal fashion pointing toward the presence of a compensating regulatory mechanism in the embryos (Fig. 2.14).

2.3.3 Microfluidic “Christmas Tree” Gradient Generator

A widely used microfluidic gradient generator design, first described by Jeon et al., involves a network of serpentine channels interspersed between channel branch points arranged in a pyramidal or Christmas tree pattern [46]. The branch points

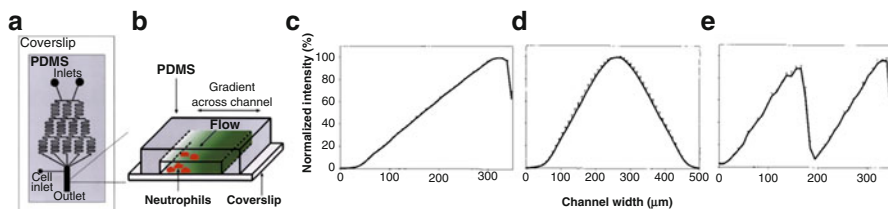


Fig. 2.15 Microfluidic Christmas tree gradient generator. **(a)** A network of serpentine channels interspersed between fluid branch points periodically split, mix, and recombine flows to develop a concentration gradient across an output channel. **(b)** Neutrophils seeded on a glass coverslip at the outlet channel are subjected to a concentration gradient across the channel. **(c)** Linear concentration gradients are readily developed and stably maintained across a 500 μm wide output channel. **(d)** Hill-shaped and **(e)** cliff-shaped gradients can be generated by placing two or more gradient generators in parallel in a head-to-head or a head-to-tail configuration, respectively. Reproduced with permission from Ref. [46]

serve to periodically split and combine flows comprising different concentrations of reagents while the serpentine channels increase the effective distance in order to ensure homogeneous mixing of flows between the branching junctions (Fig. 2.15). In this way, several different concentrations are generated on-chip, which can be directed to an output channel to produce stable spatial gradients. By adjusting the inlet concentrations, channel geometries, and flow rates, complex spatial gradient waveforms including linear and polynomial profiles can be generated. Cells are introduced in the output channel via a separate side port in order to expose them to the spatial gradient. Whitesides and colleagues used the Christmas tree gradient generator to characterize neutrophil chemotaxis in varying gradient waveforms of a soluble chemokine, IL-8. First, the authors quantified chemotactic flux in linear gradients ranging from 0 to 5, 50, and 500 ng/mL IL-8 across an output channel width of 500 μm (Fig. 2.15b). Next, the authors developed more complex hill-like and cliff-like gradient patterns by juxtaposing two gradient generators in parallel in head-to-tail (cliff) or head-to-head (hill) configurations (Fig. 2.15d, e). It was demonstrated that neutrophils encountering a gradual drop in gradient steepness (in case of a hill waveform, Fig. 2.15d) often overshoot their preferred localization zone at the region of highest concentration before returning. In contrast, a precipitous change in gradient (cliff configuration, Fig. 2.15e) revealed a tighter chemotactic control mechanism that resulted in the cells localizing at the highest concentration zone without any overshoot. It is noteworthy that bulk chemotactic assays involving concentration gradients developed in agar or agarose might have failed to detect the overshoot response of a small number of neutrophils in gradually varying spatial gradients that was observed in this study. The aforementioned gradient generator represents a cornerstone of several highly significant microfluidics-based studies on directed cell migration in tumors, stem cells, motile microbes, and leukocytes.

2.3.4 Microfluidic “Honeycomb” Chip for Antibiotic Resistance Studies

A riveting example of the application of microfluidics to create complex spatial environments is provided by the Goldilocks chip, which was developed by Robert Austin and colleagues to charter the evolution of antibiotic resistance in bacteria in a complex fitness landscape [8]. Austin’s device consisted of a honeycomb-shaped microfluidic chip with 1200 hexagonal wells etched in a silicon wafer. The wells were connected to their nearest neighbors via six microchannels, which allowed motile bacteria to travel between the wells. Nutrient and media were flowed through nanoslits etched in the side walls of the wells at the edge of the microfluidic array. A stable gradient of a genotoxic antibiotic (ciprofloxacin) was established across the array by pumping counter-flowing solutions of antibiotic-free bacterial growth media and ciprofloxacin-containing medium at the opposite peripheries of the array. GFP-labeled bacteria were inoculated at the center of the microfluidic array. It was observed that within hours of inoculation, nutrient depletion along with bacterial chemotaxis tended to concentrate an initial population of cells near the peripheries of the array where the nutrient concentration was maximum. At these so-called Goldilocks points, the stress gradients were the highest owing to the convergence of the antibiotic-free and antibiotic-containing streams. Strikingly, it was observed that antibiotic-resistant mutants fixed rapidly (within 10 h) at these Goldilocks points and eventually resulted in bacterial invasion of the entire chip. Removing the antibiotic gradient abolished emergence of resistance. Overall, the unique microfluidic approach described by Austin et al. demonstrates the alarming possibility of rapid development and fixation of antibiotic-resistant mutants in complex fitness landscapes as are likely encountered by invading pathogens in the human body [8].

2.4 Microfluidic Platforms for Drug Screening

A critical step in drug discovery and development involves the *in cellulo* toxicological and pharmacological evaluation of lead candidates [32]. In cellulo evaluation of potential therapeutics is conventionally achieved using high throughput cell culture platforms together with expensive robotic manipulations for changing media, adding reagents, and measuring cell viability or gene expression. Microfluidics holds significant promise for revolutionizing traditional drug screening by allowing assays to be conducted at physiologically relevant microscale dimensions and using ultra-low quantities of cells and test chemicals. Minimizing sample and reagent consumption is especially crucial as lead drug candidate molecules are typically available in miniscule quantities [47]. Furthermore, reduced material requirement is highly desirable for screening rare or less-readily available cell types such as patient-derived tissue constructs and hematopoietic stem cells.

Finally, as discussed in Sect. 2.1, the low form factor of microfluidic devices enables parallelization and multiplexed evaluation of several potential drugs and combinations thereof in a convenient on-chip format that has significantly less space and is cost-intensive compared to 384 or 1536 well based screens.

2.4.1 *Microfluidic Living Cell Array*

The advantages of applying microfluidic systems to drug screening are well illustrated by the microfluidic living cell array described by King et al., which enables simultaneous functional interrogation of eight cell lines individually subjected to eight different chemical stimuli (thus, a total of 64 distinct experimental conditions) (Fig. 2.16a) [48]. To enable multiplexed measurements, the living cell array utilizes a two-layered microfluidic design with the underlying fluid layer housing the cell growth chambers, which are fed by a set of eight orthogonally arranged reagent delivery channels. Each cell chamber consists of a 2×2 subarray allowing for quadruplicate measurements. Each chamber is isolated from its neighbors using two sets of valves fabricated in the control layer that rests above the fluid layer (Fig. 2.16a). In contrast to widely used actuate-to-close valves (see Sect. 2.1), King et al. employed actuate-to-open valves that can be opened by applying negative pressure in dead-end control lines (Fig. 2.16b, c). The living cell array is primed by first actuating the seeding valves and flowing in cells through eight individual cell loading lines using a syringe pump. Subsequently, the negative pressure (vacuum) applied to the seeding valves is released, which isolates the individual cell chambers. Each group of eight cell growth chambers can then be subjected to a distinct chemical stimulus by actuating a second set of stimulation control valves and flowing in the chemical reagent in a fashion analogous to cell loading (Fig. 2.16d, e). Using this approach, the authors quantified dynamic responses of rat hepatoma cell lines stably expressing GFP under the regulatory control of common eukaryotic transcription factors (NF- κ B, STAT3, GRE) and upon treatment with pro- and anti-inflammatory cytokines and dexamethasone, a steroid-based drug. Importantly, the use of actuate-to-close valves enables facile operation of the microfluidic living cell array without the need for bulky syringe pumps, which significantly improves device portability and ease-of-use.

2.4.2 *Microfluidic Antibiotic Susceptibility Testing*

We recently developed a microfluidic antibiotic susceptibility testing chip that incorporates actuate-to-open valves for screening for bacterial pathogens (Fig. 2.17) [49]. Our device consists of a 4-by-6 array of microwells in the fluid layer that can be loaded by actuating normally closed valves housed in the control layer (labeled as 1 in Fig. 2.17c, d) [49, 50]. Each well is further subdivided into two

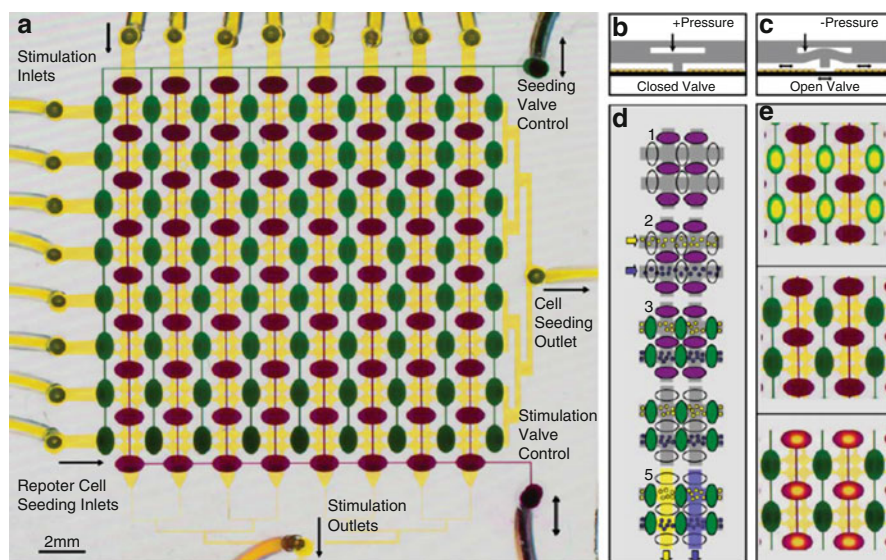


Fig. 2.16 Microfluidic living cell array. (a) The microfluidic array consists of a 16×16 array of cell growth chambers (shown in yellow) $50 \mu\text{m}$ in height and $420 \mu\text{m}$ in diameter that are supplied by eight distinct flow lines for delivering stimuli. Cells can be drawn into the chambers through eight inlets by applying negative pressure at the common outlet. Reagents or small molecule drugs can be loaded in an analogous fashion. Each 2×2 subarray of cell growth chambers can be isolated from its neighbors using two sets of control valves (shown in purple and green) fabricated in the control layer. (b) The valves are designed in an actuate-to-open configuration. In the rest state or under positive pressure, the PDMS membrane serving as the valve is in contact with the glass coverslip sealing off adjacent chambers. (c) Under the application of negative pressure, the membrane deflects upward opening the valve. (d) In *step 1*, the device is first seeded with different cell lines by releasing the cell loading valves (green) and flowing in up to eight different cell lines (*step 2*). The cell loading valves are then allowed to close isolating each cell growth chamber from its neighbors (*step 3*). After the cells are attached to the surface, the stimulus loading valves (purple) are released (*step 4*) and up to eight different reagents are flowed in to the cell chambers (*step 5*). (e) Optical micrographs of the microfluidic living cell array in the cell seeding (green cell loading valves open), neutral (all valves closed), and stimulation (purple valves open) modes of operation. Flow lines are filled with synthetic coloring to enable visual observation. Reproduced with permission from Ref. [48]

compartments isolated by a normally closed mixing valve (labeled as 2 in Fig. 2.17c, d). Cells (e.g., derived from a clinical sample such as blood or sputum) can be loaded in each of the half-wells by applying negative pressure (vacuum) to release the cell loading valves. Antibiotics can be individually loaded in the remaining four half-wells by actuating the antibiotic loading valves (similar in principle to the stimulation valves described by King et al.). Finally, actuation of the mixing valve brings the two half-wells in contact allowing the sample to be individually tested against six antibiotics in quadruplicates (Fig. 2.17d). We showed that on-chip mixing could be enhanced simply by repeated actuation of the mixing valve (to introduce eddies) thereby obviating the need for complex microfluidic

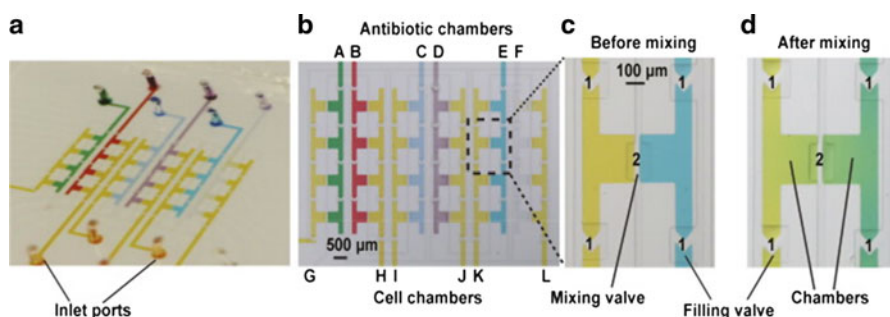


Fig. 2.17 Microfluidic antibiotic susceptibility testing (AST) chip. (a) The AST chip consists of a 4×6 array of wells that can be loaded with cells and reagents using actuate-to-open valves. (b) Each chamber is further subdivided in two chambers that are (c) separated by a valve (labeled 2) that is closed at rest. The loading valves used for seeding cells and adding media/antibiotics are labeled as 1. Adjacent chambers are loaded with cells (chambers in flow lines G–L) and antibiotics (chambers in flow lines A–F). (d) Actuation of the valve separating the cell and antibiotic chambers is achieved by applying negative pressure, which results in mixing of the contents of the adjacent wells. Reproduced with permission from Ref. [49]

mixers. Using this simple device design, we were able to infer microbial antibiotic resistance profiles (also known as antibiograms) by quantifying the expression of GEP in *E. coli* cells treated with various antibiotics and antibiotic combinations [49]. Strikingly, microfluidic implementation of antibiotic susceptibility testing enabled a tenfold improvement in turnaround time and a greater than 10^4 fold improvement in sensitivity compared to current macroscale antibiotic susceptibility testing methods. In addition, we demonstrated that antibiotic action is not strictly synergistic as a combination of multiple antibiotics does not necessarily translate to improved bactericidal activity [49]. From a clinical standpoint, the finding is significant as it implies that therapeutic interventions involving the use of multiple antibiotics in case of drug resistant infections may not always prove effective.

2.4.3 Organ-on-a-Chip Platforms for Drug Screening

Recently, microfluidic organ-on-a-chip devices have been garnering increasing attention as potential test beds for pharmacokinetic and pharmacodynamic (PK/PD) modeling of drug candidates. In their simplest form, organ-on-a-chip microfluidics seeks to simulate the physiological distribution of a drug molecule within various tissue compartments along with the pharmacological effects of the drug on the tissue of interest. To achieve this, microfluidic chambers are constructed to mimic tissues of interest (such as the liver, lungs, bone marrow, tumor) with respect to conservation of liquid residence times and volumetric ratios of the various organs. The compartments are then seeded with a physiologically relevant density of a specific cell type (e.g., hepatic cells for liver-on-a-chip)

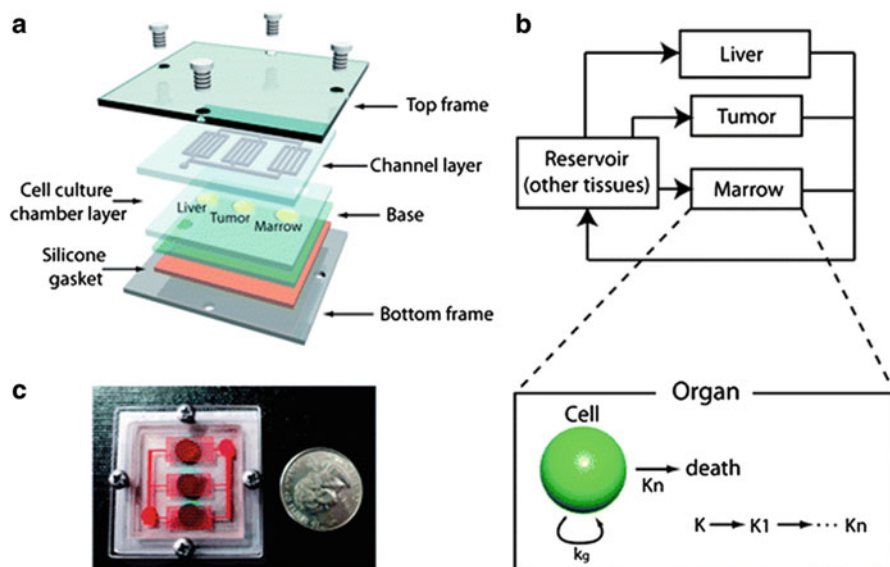


Fig. 2.18 Microfluidic cell culture analog (μ CCA). (a) The multilayer μ CCA is assembled by sealing a PDMS layer housing flow lines over a cell culture chamber. (b) Chambers and flow lines are designed to mimic the distribution of fluid flow (and drug) between the various tissue types as well as the pharmacodynamic effect of the drug on a specific tissue type. (c) The final assembled device is small, portable, and can be operated without the need for syringe pumps or vacuum manifolds. Reproduced with permission from Ref. [52]

[32, 51]. The tissue-mimetic compartments are interconnected using microfluidic channels designed to simulate physiological rates of fluid transfer between various organs. Laminar flow rates ensure that the shear stress experienced by cells was well within physiological levels ($<2 \text{ dyn cm}^{-2}$). In this way, the action of a candidate drug molecule on target cells in the chip is affected by its absorption, distribution, and metabolism within the various organ mimetic compartments, thereby providing a reasonably accurate representation of the drug's PK/PD parameters. For example, the micro-cell culture analog (μ CCA) designed by Shuler and colleagues simulates three organs on a chip: liver, a colon tumor, and bone marrow (Fig. 2.18) [52]. Each tissue type is represented by a micro-compartment that is molded in silicone and seeded with cells encapsulated in a hydrogel matrix. The cell-loaded silicone layer is sealed against a PDMS layer that houses flow lines for delivering media and drugs to the individual cell growth chambers. The flow lines are constructed to mimic the relative partitioning of blood between the tumor, liver, and bone marrow (24, 58, and 18 %, respectively). Reservoirs containing pure media are located on the chip and fluid flow within and between compartments is achieved using gravity-induced flow developed by periodically tilting the microfluidic chip on a rocking platform. By avoiding the use of external pumps and pneumatic valves, the authors improve usability and portability of the platform

as well as eliminate the notorious problem posed by air bubble formation in flow lines. Shuler and coworkers employed their microfluidic device to quantify the PK/PD profiles of a chemotherapeutic (5-fluorouracil) on the colon cancer cell lines. Moving ahead, one can envision that microfluidic systems such as these could serve as critical platforms for early stage drug testing in a PK/PD-based manner, thereby avoiding the high attrition rates and consequent economic burden associated with the drug discovery pipeline.

In summary, the simple microfluidic platforms described in this section underscore several key advantages of microfluidic cell culture arrays for drug testing, including rapid assaying of different drugs with single cell sensitivity and under physiologically relevant conditions in a convenient microchip format ($\sim 1 \text{ cm}^2$ working area) using only a few microliters of the drug or the sample. Looking ahead, microfluidic screening chips would be immensely beneficial for preclinical drug screening applications, particularly in cases where sample and/or reagent consumption needs to be minimized (as in the case for lead drug candidates or clinical specimens) as well as for field deployment of microfluidic screening devices.

2.5 Microfluidic Technologies for Single Cell Isolation and Analysis

Selective isolation and analysis of single cells has remained a long-standing challenge for sorting and studying rare cell types such as circulating tumor cells (CTCs), fetal cells in maternal blood, and drug-resistant microbial persister cells [9, 53, 54]. The ability to isolate and profile single cells also underpins escalating efforts aimed at identifying and genotyping unculturable microbes from microbiome collections. In contrast to macroscale sorting technologies, microfluidics affords three key advantages for analyzing complex consortia to isolate infrequently occurring cell types: (1) microfluidic platforms are ideal for handling small sample volumes that are typically obtained from clinical biopsies and environmental sample collections, (2) nanoliter-scale volumes of microfluidic chambers combined with the ability to integrate several thousands of wells on a single chip enables stochastic partitioning of individual cells from the parent population, and (3) the isolation of single cells in nanoliter-sized wells greatly improves the speed and sensitivity of analytical biochemical reactions such as PCR and FISH.

2.5.1 *Microfluidic Platforms for Isolating “Rare” Eukaryotic Cells*

Rare eukaryotic cells such as fetal cells in maternal blood, drug-resistant hematopoietic stem cells in chronic myeloid leukemia patients, and circulating tumor cells (CTCs) in cancer patients comprise between 10^{-4} and 10^{-7} % of the total cell

population in blood. Nevertheless, these rare cells are of tremendous diagnostic and prognostic significance, respectively for prenatal diagnosis and for predicting metastatic burden in cancer patients. Microfluidics has recently emerged as a valuable platform for isolating and profiling clinically and therapeutically relevant rare eukaryotic cells.

2.5.1.1 Microfluidic CTC Isolation Platforms

CTCs are responsible for establishing metastatic tumors at sites secondary to the primary tumor and are recognized as the major cause of mortality in cancer patients. For this reason, improved methods for the isolation and characterization of CTCs from patient whole blood are critically required. The low concentration of CTCs, however, makes their detection extremely challenging. Furthermore, even CTCs originating from the same primary tumor vary considerably in their metastatic potential and proteomic profiles, which highlights the need for single cell profiling. To this end, several microfluidic platforms have been described for achieving isolation of pure CTCs [10, 11, 55]. Here, we focus on the CTC chip described by Toner and colleagues and a more recent integrated CTC-secretome profiling microfluidic device described by Shi and coworkers.

The CTC chip, described by Toner et al., features a dense array of 78,000 microposts (100 μm in height and width) engraved using deep reactive ion etching (DRIE) on a silicon wafer with an effective surface area of 970 mm^2 (Fig. 2.19) [10]. The microposts are chemically functionalized with anti-epithelial cell adhesion molecule (EpCAM) antibodies to facilitate affinity capture of CTCs, which are known to overexpress the EpCAM cell surface antigen (Fig. 2.19d). The chip design was informed by model-guided simulations and optimized to maximize contact time between the CTCs and the capture antibodies as well as minimize shear stress at the microposts, which is detrimental to CTC adhesion. Accordingly, an equilateral triangle arrangement of microposts was employed and shown to reduce the shear stress to 0.4 dyn cm^{-2} for a volumetric flow rate of 1 mL h^{-1} , thereby maximizing CTC capture with minimal shear-induced cell damage. Using the optimized design, the authors successfully identified CTCs in 115 patient blood samples in concentrations ranging from 5 to 1281 CTCs per mL of whole blood and with purities of 52–67 % as determined by CTC-specific antibody staining. Interestingly, the high sensitivity of the CTC chip enabled identification of CTCs in patients with clinically localized prostate cancer vis-à-vis metastatic prostate cancer. Importantly, the isolated CTCs could be used for off-chip biochemical analysis via immunostaining for cancer biomarkers (such as the prostate-specific antigen) and RT PCR. The CTC chip outcores immunomagnetic bead-based isolation methods commonly used in clinical applications in terms of the former's high sensitivity (1 in 10^9 cells), specificity (an improvement of two orders of magnitude), and overall CTC yield (99 %). It is conceivable that in coming years, CTC chip would become the platform of choice for detecting metastatic cancers and

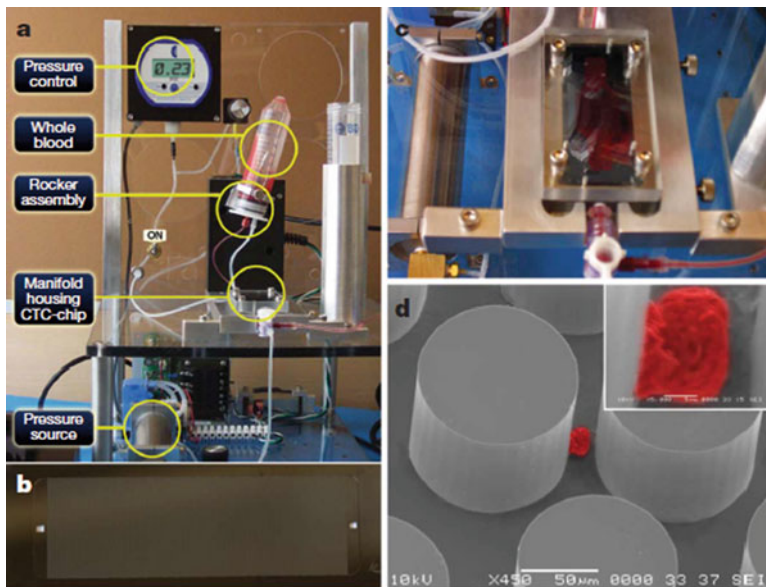


Fig. 2.19 Microfluidic CTC chip. (a) Circulating tumor cells are isolated using a simple workstation in which whole blood (mixed continuously on a rocking platform) is pumped through the chip (shown in b) using pressure-driven flow. (c) Whole blood-loaded chip. (d) Scanning electron micrograph of the CTC chip showing a lung cancer cell captured at an anti-EpCAM functionalized post. Reproduced with permission from Ref. [10]

monitoring treatment progression, thereby obviating the need for cumbersome tissue biopsies.

Shi and colleagues recently described a highly integrated microfluidic device for the isolation and secretomic profiling of CTCs (Fig. 2.20) [11]. Fabricated as a multicomponent glass-PDMS multilayer chip, the device combines four previously described microfluidic designs to achieve integrated CTC isolation and analysis, including selective isolation of CTCs, size-based removal of the smaller red blood cells, immunomagnetic removal of leukocytes and granulocytes, and single cell bar coding of the isolated CTCs to detect secreted cytokines (secretome profiling). For the isolation of CTCs from blood, CTCs were selectively labeled using anti-EpCAM antibodies (analogous to the capture antibody described above) that were chemically conjugated to single-stranded DNA (ssDNA) using a photocleavable linker. ssDNA-encoded antibody labeled cells were then affinity-captured by flowing the samples through a microfluidic channel functionalized with complementary ssDNA. DNA hybridization was enhanced by incorporating a herringbone chip design that maximized mixing by generating microvortices (Fig. 2.20b–d). Erythrocytes were removed via size-based exclusion by flowing the samples through spiral microfluidic channels. White blood cells were removed using on-chip immunomagnetic pull-down, and CTCs were released from the ssDNA capture probes using brief UV illumination to cleave the photolabile linker. Finally,

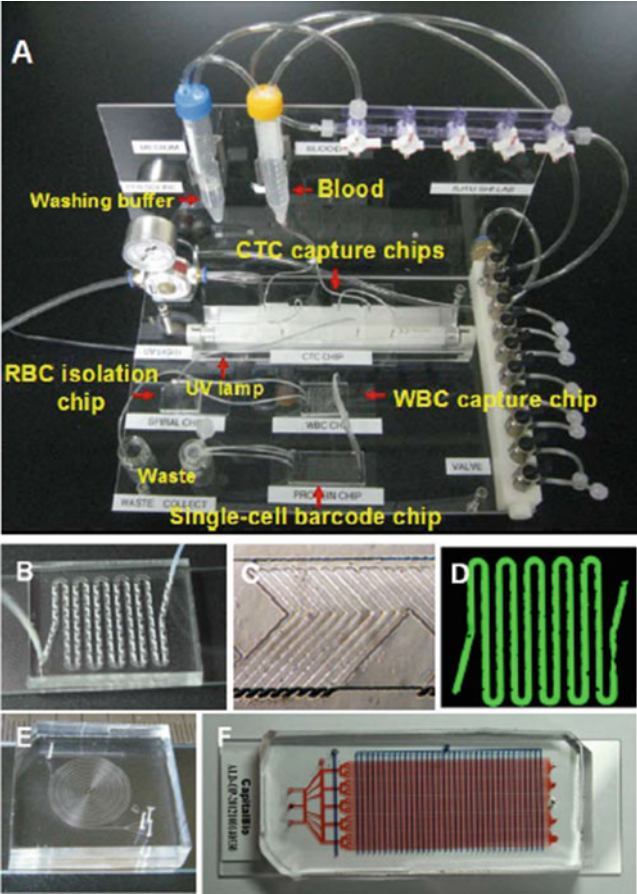


Fig. 2.20 Microfluidic CTC isolation and secretome analysis workstation. **(a)** The integrated CTC chip isolates CTC(s) from whole blood, while removing RBC(s) and WBC(s) and routes the CTC (s) to a single cell barcoding chip for analyzing secreted proteins. **(b–d)** Herringbone patterns on the chip generate microvortices, which improve efficiency of ssDNA hybridization-mediated capture of CTC(s). Hybridized DNA (fluorescently tagged) is shown in **(d)** and indicates a high density of DNA patterning on-chip. **(e)** A size-exclusion spiral chip is used to separate out the RBC (s). **(f)** The single cell barcoding chip is basically an array of single cell isolation compartments that are patterned with a panel of antibodies to identify the proteins secreted by the trapped cell. Reproduced with permission from Ref. [11]

the released CTCs were routed to a single cell bar coding (SCBC) microfluidic chamber for secretomic profiling (Fig. 2.20f). The SCBC, first described by Heath and colleagues [56], is a microfluidic device consisting of an array of microchambers (1 nL volume per chamber) for isolating single cells. Each microchamber also contains a micropatterned antibody barcode attached to the surface via DNA hybridization. CTCs are loaded and partitioned between the antibody barcoded chambers following Poisson statistics (<2 cells per chamber).

Poly-L-lysine coating of the glass layer improves CTC retention in a nanochamber. Following cell culture, the secreted proteins are immobilized at the specific antibody sites in each reaction chamber. Detection is achieved by loading the nanochambers with biotinylated secondary antibodies and probing with streptavidin-conjugated fluorophores. In this way, each CTC is quantitatively barcoded in terms of its secretome. The small volume of the reaction chambers coupled with the high efficiency of antibody capture enables the detection of secreted cytokines with exquisite sensitivity and specificity. Using this approach, the authors demonstrated a high degree of heterogeneity between secreted levels of IL-8 and VEGF among CTCs isolated from the blood of a cancer patient.

2.5.1.2 Microfluidics for Monoclonal Antibody Production

As a final example of the burgeoning importance of microfluidics for the isolation and analysis of single eukaryotic cells, we describe the application of microfluidic platforms for antibody production and screening. Monoclonal antibodies are high-value bioproducts as therapeutics in a broad range of diseases. Current antibody production technologies, however, generate polyclonal mixtures of antibody-secreting hybridomas, which need to be laboriously screened to isolate the clone producing the antibody of interest. Furthermore, during the lengthy screening and clonal expansion process, clones of interest that produce the desired antibody are often outcompeted by other members of the polyclonal consortia that have faster growth rates. Love and colleagues addressed this challenge by developing a PDMS-based microfluidic platform comprising 25,000 micro-engraved wells, each 100 μm in diameter and height and spaced 100 μm apart from neighboring wells [57]. The wells were loaded by pipetting a dilute suspension of mouse hybridomas on the surface of the microwell array and letting it sit for 3 min. Poissonian partitioning of the cells ensured that the majority of the wells received between 0 and 3 cells. Excess liquid was removed using filter papers, and the microfluidic array was inverted and clamped against a glass slide and incubated at 37 $^{\circ}\text{C}$ for a few hours. The glass slide was pretreated and covalently functionalized with antigens specific to the antibody of interest. Under these conditions, antibodies secreted by cells in each microwell will adhere to the glass substrate only if it is specific to the antigen coating of the glass substrate. Detection is achieved using fluorescently labeled secondary antibodies and the glass slide is scanned using a microarray scanner to identify the location of the fluorescent signal, which is spatially registered with the corresponding antibody secreting monoclonal cell bearing microwell (Fig. 2.21). Following detection, the hybridoma cells of interest can be clonally expanded for scaling up antibody production. In this way, a relatively simple microfluidic platform (single layer and without valves, mixers, and pumps, fluid loading by pipetting) greatly simplified a long-standing challenge for therapeutic antibody production [57].

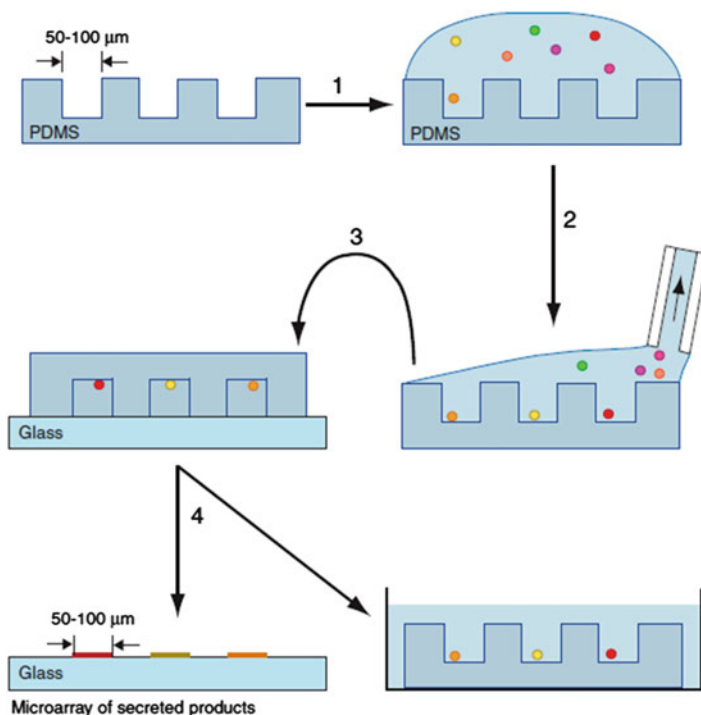


Fig. 2.21 Microfluidic hybridoma screening chip. A microfluidic array of wells enabled the isolation of single hybridoma cells based on Poisson partitioning. The seeded microfluidic array was dewetted using a filter paper and inverted over a glass slide functionalized with antibodies to detect a secreted antigen of interest. The glass slides were scanned using a microarray scanner to identify the spatial position corresponding to the hybridoma secreting an antibody of interest. Following detection, the hybridoma chip can be reused for detecting additional antigen producing cells as well as to scale up production. Reproduced with permission from Ref. [57]

2.5.2 Isolation and Genetic Analysis of Uncultivated Microbes

It is estimated that the vast majority of microorganisms are not amenable to laboratory-scale cultivation techniques that frequently fail to faithfully replicate the microbe's native niche (e.g., a nontrivial dependence on host-derived factors) [54]. In addition, cultivation of heterogeneous microbial consortia usually selects for fast-growing strains, which rapidly outcompete other species. Unculturable microbes, sometimes referred to as biological dark matter, represent an untapped and poorly studied resource that is of tremendous clinical as well as industrial significance. While metagenomic sequencing enables genetic analysis of heterogeneous environmental samples, the identification of species-specific genes and genome sequences from complex metagenomic data is an intense and computationally challenging endeavor. Recently, several microfluidics-based cell isolation platforms have significantly accelerated the discovery of novel microbes from complex multispecies communities, as is described below.

2.5.2.1 Microfluidic Digital PCR Chip

Leadbetter and colleagues described a multilayer microfluidic device that was used to discern the genetic signature of a previously unknown bacterial species in the termite gut [58]. The microfluidic chip comprised 1176 nano-chambers (6.25 nL volume per chamber) separated by actuate-to-close micromechanical valves connected by a single feed line. Termite hindgut luminal contents were diluted in PCR buffer and loaded in the microfluidic chip to achieve a Poissonian distribution of cells in the chambers, thereby ensuring that the majority of chambers housed between 0 and 1 bacterial cell. Subsequent to loading, the individual chambers were isolated from each other by pneumatic or hydraulic actuation of micromechanical push up valves, which deflected the elastomeric PDMS membrane between the upper flow layer and the bottom control layer. Each chamber was then used as an independent PCR reactor to co-amplify bacterial 16 s rDNA using broad-specificity bacterial primers as well as the gene for formyltetrahydrofolate synthetase (FTHFS), which is a key metabolic enzyme involved in bacterial homoacetogenesis and hitherto unassociated with a specific species or clade in the termite hindgut microbiome. Colocalization of spectrally separated fluorescence signals derived from the amplification of bacterial rDNA as well as the FTHFS gene were used to identify microfluidic chambers housing bacterial cells encoding the FTHFS gene. PCR amplicons were retrieved using syringe needles, re-amplified, and sequenced, which revealed that all the FTHFS-encoding bacterial 16 s rRNA sequences clustered in four closely related groups within the *Spirochaete* cluster. Members of this newly identified clade were not observed in microfluidic PCR chambers that failed to amplify the FTHFS gene, suggesting that the *Spirochaete* cluster is the predominant species responsible for homoacetogenic metabolism in the termite hindgut. In this way, a relatively simple microfluidic design capable of achieving single cell confinement and digital PCR enabled the clade-specific association of a key bacterial enzyme affecting energy requirements of the microbiome's termite host.

2.5.2.2 Single Cell Genome Amplification Chip

Quake and coworkers developed a more integrated version of the microfluidic digital PCR chip detailed in the prior section in order to isolate and sequence the genome of a novel bacterial species from a human subgingival swab sample (Fig. 2.22a) [59]. The microfluidic platform integrated morphology-based cell sorting, lysis, neutralization, and whole genome amplification in a single chip. In this design, cell sorting, lysis, and neutralization chambers (each 3.5 nL in volume) along with a larger (50 nL volume) whole genome amplification (WGA) chamber are arranged sequentially and isolated from each other through the use of micromechanical valves similar to the ones described above (Fig. 2.22b). Single bacterial cells with a characteristic rod-like shape typical of the uncultivated TM7 phylum are manually identified using microscopy and mechanically trapped in the

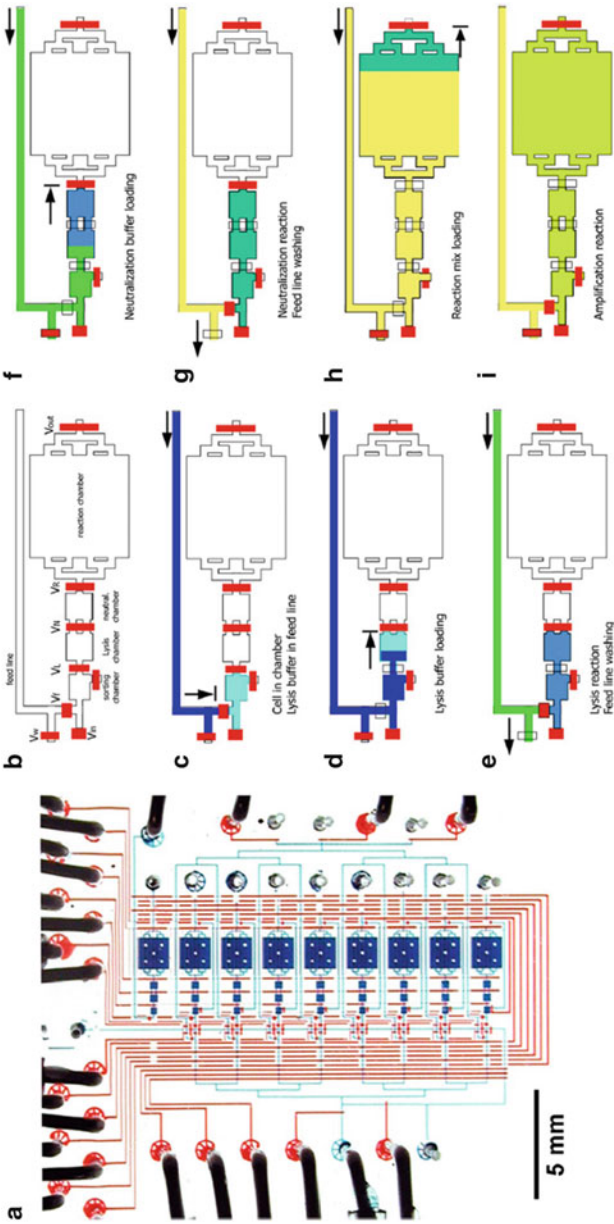


Fig. 2.22 Single cell genome amplification chip. (a) Digital image of the single cell whole genome amplification chip capable of processing eight samples in parallel. The flow and control lines are respectively filled with blue and red food coloring. (b) Each processing unit comprises separate chambers for cell sorting, lysis, neutralization, and whole genome amplification. Reagents are loaded through the feed line to the various chambers or routed to the waste line when the valve V_w is open. A single cell is introduced into the sorting chamber by opening valve V_{in} . The sorting, lysis, and neutralization chambers are separated by valves V_L , V_N , and V_R . Valve V_{out} can be opened to collect the amplified DNA directly in a microcentrifuge tube. (c) A single cell (identified based on morphology) is loaded into the sorting chamber and the feed line is filled with lysis buffer (shown in dark blue). (d) The lysis buffer is used to guide the cell into the lysis chamber by opening valve V_L . (e) As the cell is being lysed, the feed line is rinsed with buffer (by opening valve V_w). (f) Neutralization buffer (shown in green) is loaded in the feed line and used to flow the lysate into the neutralization chamber by actuating valve V_N . (g) As the lysate is neutralized, the feed line is rinsed and (h) loaded with reagents for whole genome amplification, which flows the neutralized lysate into the reaction chamber. (i) Genome from a single cell is isolated in the reaction chamber and the products collected. Reproduced with permission from Ref. [59]

sorting chamber (Fig. 2.22c). A feed line is used to deliver lysis reagents to the cell chamber and the lysis reaction mix is routed to the downstream lysis chamber via actuation of an intervening valve (Fig. 2.22d). Following lysis, the reaction mixture is neutralized (Fig. 2.22f) and routed to the reaction chamber for whole genome amplification of a single bacterial cell (Fig. 2.22h). Reagents for neutralization and genome amplification are delivered via the feed line, which is flushed in between each step by routing the washing buffer to a waste stream through the actuation of a separate valve (Fig. 2.22e, g). Amplified genomic DNA is retrieved and used for 16S rRNA sequencing to identify the clade corresponding to the isolated rod-shaped bacterium. Using microfluidic sorting, genome amplification, retrieval, and sequencing, the authors were able to assemble the genome sequence of the first representative species of the TM7 phylum.

2.5.2.3 Microfluidic “SlipChip”

Recently, Ismagilov and coworkers adapted the SlipChip microfluidic platform originally developed for protein crystallization and digital PCR to facilitate the cultivation of a representative gut microbiome species (Fig. 2.23) [60]. The SlipChip platform consists of two glass plates housing nanowells along with microfluidic channels for loading the nanowells. The two plates can be moved

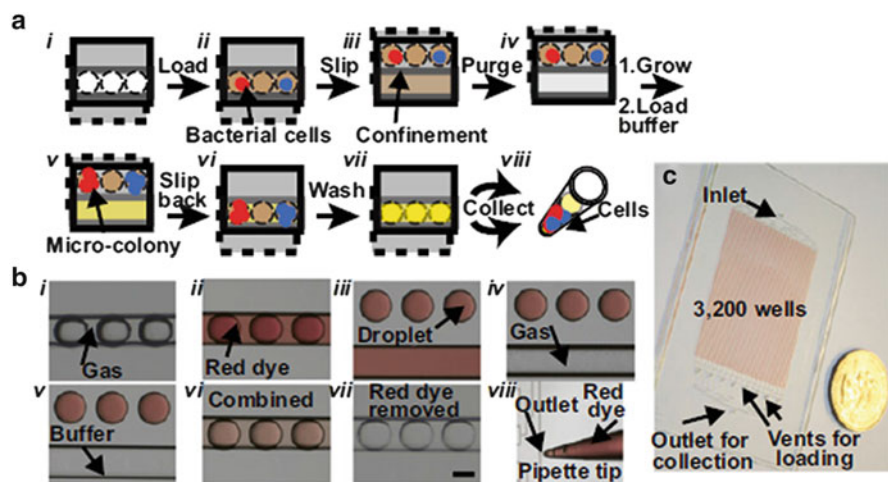


Fig. 2.23 Microfluidic SlipChip. (a) Wells engraved in one of the plates of the SlipChip can be loaded with cells by flowing a cell-loaded solution through channels engraved in the other plate. Slipping the plates relative to each other confines the cells in a microwell to form microcolonies. In order to isolate the microcolonies, the plates are slipped back again to align the channels with the wells. Colonies are collected by flowing a collection buffer through the channels. (b) Operation of the schematically illustrated steps in (a) are visualized using a red dye. (c) The SlipChip is slightly larger than a US quarter and features 3200 wells for isolating and growing single cells. Reproduced with permission from Ref. [60]

relative to one another enabling the user to (1) align the nanowells in one plate with microchannels in the other plate to accomplish well loading and (2) to bring the contents in nanowells housed in the upper plate in contact with nanowells in the lower plate to enable reagent mixing by diffusion (Fig. 2.23a, b). A key feature of the SlipChip platform is that it allows fluidic routing without the need for pumps and valves. SlipChips developed for microbial cultivation comprise approximately 3200 nanowells (6 nL volume) engraved in photoresist in a chromium-coated glass substrate (Fig. 2.23c). In a typical operation of the SlipChip, the microfluidic channels and nanowells are loaded with a bacterial sample from a clinical biopsy (e.g., from the mucosal lining of human cecum). Slipping the bottom plate relative to the upper plate results in confinement of the stochastically partitioned bacterial cells in each nanowell, following which the cells are allowed to grow and establish microcolonies. To collect the cells, the lower plate is slipped in order to realign the wells with the channel and a buffer solution is flowed through the channel to collect pooled bacterial colonies, which can be analyzed off-chip for 16S rRNA ribotyping. A key feature of the SlipChip platform is that the top and bottom plates can be separated from each other following the growth of microcolonies. In this way, bacterial populations are partitioned between nanowells in the two plates, one of which can be used for destructive genetic profiling off-chip while the other plate can be retained to enable macroscale cell cultivation based on the genotyping results, thereby providing a platform for targeted microbial cultivation. An added advantage of SlipChip is that it expedites the investigation of diverse culture conditions. This is readily achieved by slipping the bottom plate relative to the upper plate to align the nanowells in the lower plate with the channels in the upper plate, which can then be loaded with a specific conditioning reagent to facilitate cell culture. As a powerful demonstration of the potential utility of the SlipChip cell culture platform, Ma et al. employed SlipChip to cultivate the first species of the *Oscillobacter* genus (classified among the “most wanted taxa” of the human microbiome project) by conditioning the culture medium with autoclaved fluid collected from the sampling site in a human cecum [60].

2.6 Conclusions and Future Outlook

In the preceding sections, we have described several significant advances in various fields of biology that have been enabled and enhanced by microfluidic technologies. Through these examples, we have attempted to highlight key advantages of microfluidics that remain difficult or impossible to achieve using macroscale technologies—for example, single cell resolution, precise spatiotemporal control over reagent delivery, and on-chip integration of multiple steps. Nonetheless, the application of microfluidic devices for studying single cell biology is not without limitations. First, the laminar flow regime that predominates in microfluidic channels may pose a significant challenge in situations where rapid mixing is required. Efforts to circumvent diffusion-limited mixing include the incorporation of passive on-chip mixers such as herringbone grooves or serpentine channels that maximize

contact time for mixing. Second, the large surface-to-volume ratios of microfluidic devices result in enhanced absorption and adsorption of hydrophobic molecules to the PDMS surface, which can perturb the concentrations of drugs and reagents. A variety of surface passivation strategies have been described for minimizing biomolecular adhesion in microfluidic devices. Finally, despite the relative ease of replica molding techniques, soft lithography is not yet established as a routine technology in most biology laboratories. This often accounts for a certain degree of inertia in adopting microfluidic technology as an everyday tool to answer the biologist's questions [15, 24]. Several efforts to address this have been undertaken including the organization of microfluidic workshops aimed at biologists, centralized microfluidic fabrication facilities, as well as a rapidly escalating number of companies that design, develop, and deliver microfluidic chips and flow control apparatus for academic research applications. However, for microfluidics-based platforms to be adapted as everyday tools in cell and molecular biology labs, it is imperative that newer as well as established microfluidic devices are used beyond proof-of-principle experiments to tackle key challenges in systems and synthetic biology, clinical diagnostics, and applied microbiology [15, 17].

In closing, the examples described in this chapter highlight several applications and new discoveries that were uniquely enabled by microfluidics, the vast majority of which could not have been readily realized using existing macro or microscale alternatives. Taken together with escalating advances in high-throughput sequencing, transcriptome profiling, and genome editing and the development of improved genetically encoded probes for functional imaging, it is clear that microfluidics is ideally poised to address exciting new frontiers in the field of single cell biology.

References

1. Samoilov MS, Price G, Arkin AP (2006) From fluctuations to phenotypes: the physiology of noise. *Sci Signal* 2006(366):re17–re17
2. Raj A, van Oudenaarden A (2008) Nature, nurture, or chance: stochastic gene expression and its consequences. *Cell* 135(2):216–226
3. Thattai M, van Oudenaarden A (2001) Intrinsic noise in gene regulatory networks. *Proc Natl Acad Sci U S A* 98(15):8614–8619
4. Paulsson J (2004) Summing up the noise in gene networks. *Nature* 427(6973):415–418
5. Ozbudak EM, Thattai M, Kurtser I, Grossman AD, van Oudenaarden A (2002) Regulation of noise in the expression of a single gene. *Nat Genet* 31(1):69–73
6. Maamar H, Raj A, Dubnau D (2007) Noise in gene expression determines cell fate in *Bacillus subtilis*. *Science* 317(5837):526–529
7. Elowitz MB, Levine AJ, Siggia ED, Swain PS (2002) Stochastic gene expression in a single cell. *Science* 297(5584):1183–1186
8. Zhang Q et al (2011) Acceleration of emergence of bacterial antibiotic resistance in connected microenvironments. *Science* 333(6050):1764–1767
9. Balaban NQ, Merrin J, Chait R, Kowalik L, Leibler S (2004) Bacterial persistence as a phenotypic switch. *Science* 305(5690):1622–1625
10. Nagrath S et al (2007) Isolation of rare circulating tumour cells in cancer patients by microchip technology. *Nature* 450(7173):1235–1239

11. Deng Y et al (2014) An integrated microfluidic chip system for single-cell secretion profiling of rare circulating tumor cells. *Sci Rep* 4:7499
12. Shaner NC, Steinbach PA, Tsien RY (2005) A guide to choosing fluorescent proteins. *Nat Methods* 2(12):905–909
13. Mukherjee A, Schroeder CM (2015) Flavin-based fluorescent proteins: emerging paradigms in biological imaging. *Curr Opin Biotechnol* 31:16–23
14. Zare RN, Kim S (2010) Microfluidic platforms for single-cell analysis. *Annu Rev Biomed Eng* 12:187–201
15. Whitesides GM (2006) The origins and the future of microfluidics. *Nature* 442(7101):368–373
16. Gravesen P, Branebjerg J, Jensen OS (1993) Microfluidics-a review. *J Micromech Microeng* 3(4):168
17. Beebe DJ, Mensing GA, Walker GM (2002) Physics and applications of microfluidics in biology. *Annu Rev Biomed Eng* 4:261–286
18. Sia SK, Kricka LJ (2008) Microfluidics and point-of-care testing. *Lab Chip* 8(12):1982–1983
19. Kim S, Kim HJ, Jeon NL (2010) Biological applications of microfluidic gradient devices. *Integr Biol* 2(11–12):584–603
20. Breslauer DN, Lee PJ, Lee LP (2006) Microfluidics-based systems biology. *Mol Biosyst* 2(2):97–112
21. Bennett MR, Hasty J (2009) Microfluidic devices for measuring gene network dynamics in single cells. *Nat Rev Genet* 10(9):628–638
22. Toriello NM et al (2008) Integrated microfluidic bioprocessor for single-cell gene expression analysis. *Proc Natl Acad Sci U S A* 105(51):20173–20178
23. Thorsen T, Maerkl SJ, Quake SR (2002) Microfluidic large-scale integration. *Science* 298(5593):580–584
24. Whitesides GM, Ostuni E, Takayama S, Jiang X, Ingber DE (2001) Soft lithography in biology and biochemistry. *Annu Rev Biomed Eng* 3(1):335–373
25. Sia SK, Whitesides GM (2003) Microfluidic devices fabricated in poly(dimethylsiloxane) for biological studies. *Electrophoresis* 24(21):3563–3576
26. McDonald JC, Whitesides GM (2002) Poly(dimethylsiloxane) as a material for fabricating microfluidic devices. *Acc Chem Res* 35(7):491–499
27. Berthier E, Young EW, Beebe D (2012) Engineers are from PDMS-land, biologists are from polystyrenia. *Lab Chip* 12(7):1224–1237
28. Unger MA, Chou H-P, Thorsen T, Scherer A, Quake SR (2000) Monolithic microfabricated valves and pumps by multilayer soft lithography. *Science* 288(5463):113–116
29. Suh YK, Kang S (2010) A review on mixing in microfluidics. *Micromachines* 1(3):82–111
30. de Jong J, Lammertink RG, Wessling M (2006) Membranes and microfluidics: a review. *Lab Chip* 6(9):1125–1139
31. Grover WH, Ivester RH, Jensen EC, Mathies RA (2006) Development and multiplexed control of latching pneumatic valves using microfluidic logical structures. *Lab Chip* 6(5):623–631
32. Dittrich PS, Manz A (2006) Lab-on-a-chip: microfluidics in drug discovery. *Nat Rev Drug Discov* 5(3):210–218
33. Bennett MR et al (2008) Metabolic gene regulation in a dynamically changing environment. *Nature* 454(7208):1119–1122
34. Balagaddé FK, You L, Hansen CL, Arnold FH, Quake SR (2005) Long-term monitoring of bacteria undergoing programmed population control in a microchemostat. *Science* 309(5731):137–140
35. Di Carlo D, Aghdam N, Lee LP (2006) Single-cell enzyme concentrations, kinetics, and inhibition analysis using high-density hydrodynamic cell isolation arrays. *Anal Chem* 78(14):4925–4930
36. Ryley J, Pereira-Smith OM (2006) Microfluidics device for single cell gene expression analysis in *Saccharomyces cerevisiae*. *Yeast* 23(14–15):1065–1073
37. Tanyeri M, Ranka M, Sittipolkul N, Schroeder CM (2011) A microfluidic-based hydrodynamic trap: design and implementation. *Lab Chip* 11(10):1786–1794

38. Tanyeri M, Johnson-Chavarria EM, Schroeder CM (2010) Hydrodynamic trap for single particles and cells. *Appl Phys Lett* 96(22):224101
39. Johnson-Chavarria EM, Agrawal U, Tanyeri M, Kuhlman TE, Schroeder CM (2014) Automated single cell microbioreactor for monitoring intracellular dynamics and cell growth in free solution. *Lab Chip* 14(15):2688–2697
40. Lucchetta EM, Lee JH, Fu LA, Patel NH, Ismagilov RF (2005) Dynamics of *Drosophila* embryonic patterning network perturbed in space and time using microfluidics. *Nature* 434(7037):1134–1138
41. Levorio TJ, Zhan M, Lim B, Shvartsman SY, Lu H (2013) Microfluidic trap array for massively parallel imaging of *Drosophila* embryos. *Nat Protoc* 8(4):721–736
42. Chung K et al (2011) A microfluidic array for large-scale ordering and orientation of embryos. *Nat Methods* 8(2):171–176
43. Chronis N, Zimmer M, Bargmann CI (2007) Microfluidics for in vivo imaging of neuronal and behavioral activity in *Caenorhabditis elegans*. *Nat Methods* 4(9):727–731
44. Takayama S et al (2003) Selective chemical treatment of cellular microdomains using multiple laminar streams. *Chem Biol* 10(2):123–130
45. Takayama S et al (2001) Laminar flows: subcellular positioning of small molecules. *Nature* 411(6841):1016–1016
46. Li Jeon N et al (2002) Neutrophil chemotaxis in linear and complex gradients of interleukin-8 formed in a microfabricated device. *Nat Biotechnol* 20(8):826–830
47. Thorson MR et al (2011) A microfluidic platform for pharmaceutical salt screening. *Lab Chip* 11(22):3829–3837
48. King KR et al (2007) A high-throughput microfluidic real-time gene expression living cell array. *Lab Chip* 7(1):77–85
49. Mohan R et al (2013) A multiplexed microfluidic platform for rapid antibiotic susceptibility testing. *Biosens Bioelectron* 49:118–125
50. Schudel BR, Tanyeri M, Mukherjee A, Schroeder CM, Kenis PJ (2011) Multiplexed detection of nucleic acids in a combinatorial screening chip. *Lab Chip* 11(11):1916–1923
51. Sin A et al (2004) The design and fabrication of three-chamber microscale cell culture analog devices with integrated dissolved oxygen sensors. *Biotechnol Prog* 20(1):338–345
52. Sung JH, Kam C, Shuler ML (2010) A microfluidic device for a pharmacokinetic-pharmacodynamic (PK-PD) model on a chip. *Lab Chip* 10(4):446–455
53. Hou HW et al (2011) Microfluidic devices for blood fractionation. *Micromachines* 2(4):319–343
54. Vincent ME, Liu W, Haney EB, Ismagilov RF (2010) Microfluidic stochastic confinement enhances analysis of rare cells by isolating cells and creating high density environments for control of diffusible signals. *Chem Soc Rev* 39(3):974–984
55. Gleghorn JP et al (2010) Capture of circulating tumor cells from whole blood of prostate cancer patients using geometrically enhanced differential immunocapture (GEDI) and a prostate-specific antibody. *Lab Chip* 10(1):27–29
56. Ma C et al (2011) A clinical microchip for evaluation of single immune cells reveals high functional heterogeneity in phenotypically similar T cells. *Nat Med* 17(6):738–743
57. Love JC, Ronan JL, Grotenbreg GM, van der Veen AG, Ploegh HL (2006) A microengraving method for rapid selection of single cells producing antigen-specific antibodies. *Nat Biotechnol* 24(6):703–707
58. Ottesen EA, Hong JW, Quake SR, Leadbetter JR (2006) Microfluidic digital PCR enables multigene analysis of individual environmental bacteria. *Science* 314(5804):1464–1467
59. Marcy Y et al (2007) Dissecting biological “dark matter” with single-cell genetic analysis of rare and uncultivated TM7 microbes from the human mouth. *Proc Natl Acad Sci U S A* 104(29):11889–11894
60. Ma L et al (2014) Gene-targeted microfluidic cultivation validated by isolation of a gut bacterium listed in Human Microbiome Project’s Most Wanted taxa. *Proc Natl Acad Sci* 111(27):9768–9773

Microfluidic Methods for Molecular Biology

Lu, C.; Verbridge, S.S. (Eds.)

2016, XII, 376 p. 137 illus., 118 illus. in color.,

Hardcover

ISBN: 978-3-319-30017-7